Received: 19 July 2019 | Revised: 8 October 2019 | Accepted: 21 October 2019

DOI: 10.1096/fj.201901817R

RESEARCH ARTICLE

THE FASEB JOURNAL

An adipose tissue galectin controls endothelial cell function via preferential recognition of 3-fucosylated glycans

Sebastián M. Maller[1,2] | Alejandro J. Cagnoni[1] | Nadia Bannoud[3] | Lorena Sigaut[4] | Juan M. Pérez Sáez[2] | Lía I. Pietrasanta[4,5] | Ri-Yao Yang[6] | Fu-Tong Liu[7] | Diego O. Croci[3,8] | Santiago Di Lella[9,10] | Victoria Sundblad[2] | Gabriel A. Rabinovich[2,10] | Karina V. Mariño[1]

[1]Laboratorio de Glicómica Funcional y Molecular, Instituto de Biología y Medicina Experimental, Consejo Nacional de Investigaciones Científicas y Técnicas (IBYME-CONICET), Buenos Aires, Argentina

[2]Laboratorio de Inmunopatología, Instituto de Biología y Medicina Experimental, Consejo Nacional de Investigaciones Científicas y Técnicas (IBYME-CONICET), Buenos Aires, Argentina

[3]Laboratorio de Inmunopatología, Facultad de Ciencias Médicas, Instituto de Histología y Embriología de Mendoza (IHEM), Consejo Nacional de Investigaciones Científicas y Técnicas (CONICET), Universidad Nacional de Cuyo, Mendoza, Argentina

[4]Departamento de Física, Facultad de Ciencias Exactas y Naturales, Universidad de Buenos Aires and Instituto de Física de Buenos Aires (IFIBA-CONICET), Buenos Aires, Argentina

[5]Centro de Microscopías Avanzadas (CMA), Facultad de Ciencias Exactas y Naturales, Universidad de Buenos Aires, Buenos Aires, Argentina

[6]Department of Molecular and Cellular Oncology, The University of Texas MD Anderson Cancer Center, Houston, Texas

[7]Institute of Biomedical Sciences, Academia Sinica, Taipei, Taiwan

[8]Facultad de Ciencias Exactas y Naturales, Universidad Nacional de Cuyo, Mendoza, Argentina

[9]Instituto de Química Biológica, Ciencias Exactas y Naturales (IQUIBICEN-CONICET), Buenos Aires, Argentina

[10]Departamento de Química Biológica, Facultad de Ciencias Exactas y Naturales, Universidad de Buenos Aires, Buenos Aires, Argentina

Correspondence
Gabriel A. Rabinovich, Laboratorio de Inmunopatología, Instituto de Biología y Medicina Experimental, Consejo Nacional de Investigaciones Científicas y Técnicas (IBYME-CONICET), Buenos Aires C1428ADN, Argentina.
Email: gabriel.r@ibyme.conicet.gov.ar, gabyrabi@gmail.com

Karina V. Mariño, Laboratorio de Glicómica Funcional y Molecular, Instituto de Biología y Medicina Experimental, Consejo Nacional de Investigaciones Científicas y Técnicas (IBYME-CONICET), Buenos Aires C1428ADN, Argentina.
Email: kmarino@ibyme.conicet.gov.ar

Abstract

Upon overnutrition, adipocytes activate a homeostatic program to adjust anabolic pressure. An inflammatory response enables adipose tissue (AT) expansion with concomitant enlargement of its capillary network, and reduces energy storage by increasing insulin resistance. Galectin-12 (Gal-12), an endogenous lectin preferentially expressed in AT, plays a key role in adipocyte differentiation, lipolysis, and glucose homeostasis. Here, we reveal biochemical and biophysical determinants of Gal-12 structure, including its preferential recognition of 3-fucosylated structures, a unique feature among members of the galectin family. Furthermore, we identify a previously unanticipated role for this lectin in the regulation of angiogenesis within AT. Gal-12 showed preferential localization within the inner side of lipid droplets, and its expression was upregulated under hypoxic conditions. Through glycosylation-dependent binding to endothelial cells, Gal-12 promoted in vitro angiogenesis.

Abbreviations: ASF, asialofetuin; CRD, carbohydrate recognition domain; DOC, 3α-12α-dihydroxy-5β-cholanic acid sodium salt; FCS, fetal calf serum; Gal, galectin; HA, hemagglutination assay; HIA, hemagglutination inhibition assay; IBMX, isobutyl-methyl-xanthine; IPTG, isopropyl β-D-1-thiogalactopyranoside; ITC, isothermal titration calorimetry; LB, lysogeny broth; LBG, ligand-binding groove; LD, lipid droplet; ORF, open reading frame; PMSF, phenylmethylsulfonyl fluoride; RBC, red blood cells; SPA, solid phase assay; TLCK, *N*-α-tosyl-*L*-lysine chloromethyl ketone hydrochloride; TMB, tetramethylbenzidine.

© 2019 Federation of American Societies for Experimental Biology

Funding information
CONICET; Sales Foundation; Bunge & Born Foundation; René Barón Foundation; The Richard Lounsbery Foundation (USA); Agencia Nacional de Promoción Científica y Tecnológica, Grant/Award Number: PICT 2015-0564, PICT V 2014-3687 and PICT 2016-0205; The University of Buenos Aires, Grant/Award Number: 20020120100276; 2013-2015

Moreover, analysis of in vivo AT vasculature showed reduced vascular networks in Gal-12-deficient (*Lgals12*$^{-/-}$) compared to wild-type mice, supporting a role for this lectin in AT angiogenesis. In conclusion, this study unveils biochemical, topological, and functional features of a hypoxia-regulated galectin in AT, which modulates endothelial cell function through recognition of 3-fucosylated glycans. Thus, glycosylation-dependent programs may control AT homeostasis by modulating endothelial cell biology with critical implications in metabolic disorders and inflammation.

KEYWORDS
adipose tissue, angiogenesis, galectins, glycosylation

1 | INTRODUCTION

Once considered merely fatty acid storage, adipose tissue (AT) is not only a key player in the regulation of energy balance but also a highly vascularized immunological organ, able to release a myriad of cytokines and adipokines, thus shaping metabolism through paracrine and endocrine mechanisms.[1] Adipocytes are the main cell type in AT and have primary roles in controlling energy homeostasis. At high nutritional states, these cells increase fatty acid uptake and store large amounts of triacylglycerol in intracellular lipid droplets (LD), whereas in demand for nutrients, LDs are shrunk by means of lipolysis.[2] The continuous advance of obesity and its associated comorbidity entities (type 2 diabetes, cancer, and cardiovascular disease, among others) places AT in the spotlight. Accumulating evidence suggest that prolonged AT remodeling in response to caloric excess leads to chronic inflammation at the expense of reduced insulin sensitivity.[1,3] Moreover, in response to over nutrition, expansion of adipocytes induces local tissue hypoxia, which, in turn, leads to expression and secretion of several pro-angiogenic factors.[4] An improved understanding of the molecular mediators linking sustained AT growth and expansion of capillary networks may reveal clinically relevant pathways through which obesity leads to metabolic diseases.

Galectins are a family of glycan-binding proteins characterized by the presence of a conserved carbohydrate recognition domain (CRD) which typically recognizes the *N*-acetyllactosamine (LacNAc; Galβ1-4GlcNAc) disaccharide.[5] The galectin (Gal) family plays key roles in immune and vascular signaling programs, either through interaction with glycosylated receptors within the extracellular milieu or by controlling intracellular signaling pathways.[6-8] Despite their lack of a classical secretory signal, galectins are found within the extracellular compartment, probably released through an unusual route that requires intact carbohydrate-binding activity of the secreted protein. By interacting with cell surface glycoconjugates, these lectins control a myriad of cellular processes including endocytosis and cell signaling cascades, leading to regulation of cellular activation, proliferation, migration, and survival.[9] Intracellularly, galectins may control a plethora of processes through protein-protein or protein-glycan interactions, including pre-RNA splicing, and energy metabolism.[10] Based on their molecular architecture, galectins have been classified into three different structural groups: (i) proto-type galectins (Gal-1, -2, -5, -7, -10, and -11), which contain a single CRD and are capable of dimerization; (ii) chimera-type galectins exhibiting a single CRD, able to form pentamers (Gal-3); and (iii) tandem-repeat type galectins, which present two CRDs of different nature within the same polypeptidic chain (Gal-4, -8, -9, and -12).[11,12] Glycan specificity of each member of the family is dictated by differences in the architecture and dynamics of the ligand-binding groove (LBG).[13,14]

While some galectins are widely expressed among different tissues, other family members have a more restricted localization.[15] Whereas Gal-1 is a pro-resolving and pro-angiogenic protein ubiquitously expressed in various cells and tissues,[7,16,17] Gal-12 is a tandem-repeat type galectin preferentially expressed in AT.[18,19]

First described in 2001,[19,20] Gal-12 exhibits two CRDs separated by a linker sequence. Notably, while its N-terminal CRD presents significant homology to that of other galectin members, including the key amino acid residues responsible for carbohydrate recognition, its C-terminal domain differs considerably from the family consensus sequence. From a biological perspective, Gal-12 is a major regulator of adipocyte differentiation.[18] In addition, a role for this lectin in the pathogenesis of insulin resistance has been postulated.[19,21] Subsequent studies demonstrated that Gal-12 is involved in regulation of lipid metabolism and energy balance.[22,23] Primarily localized in LDs, this galectin functions as a negative regulator of lipolysis, through the control of lipolytic protein kinase A signaling.[22] Interestingly, Gal-12-deficient (*Lgals12*$^{-/-}$) mice show enhanced adipocyte lipolysis and mitochondria

respiration, reduced adiposity, and ameliorated insulin resistance.[22] Of note, Gal-12 expression is not only restricted to adipocytes, as it has been also identified in macrophages, contributing to polarization of these cells toward a M1 proinflammatory profile.[23] Moreover, conditioned media from *Lgals12*$^{-/-}$ macrophages improved insulin sensitivity in adipocytes,[23] suggesting a potential role of this protein in adipocyte-macrophage cross-talk. In this context, Gal-12 emerges as a potential mediator that could bridge AT expansion, inflammation, and metabolic disease.

Remarkably, one of the main constraints that hindered biophysical and functional characterization of Gal-12 was the lack of recombinant protein. In this regard, affinity studies using recombinant Gal-12 will facilitate discovery of potential ligands for this lectin, identification of critical functions, and development of specific inhibitors. Herein, we report the expression and purification of recombinant Gal-12, as well as the molecular modeling and biochemical characterization of this lectin, including its glycan affinity and binding preferences. In addition, using the recombinant protein, glycan inhibitors, and adipose tissue from *Lgals12*$^{-/-}$ mice, we identify a novel role of this protein in the control of endothelial cell biology.

2 | MATERIALS AND METHODS

2.1 | Molecular modeling of Gal-12N and Gal-12C

The coding sequence for *Mus musculus* Gal-12 (mGal12) has been previously described (945 bp, GeneID: 56072, SeqRNA ID: NM_019516).[20] This protein has two isoforms in mice (uniprot ID: Q91VD1-1/2). In the present work, we used the full-length version, isoform-1 (uniprot ID: Q91VD1-1) of murine Gal-12.

The primary sequence for Gal-12 (isoform 1, 314 amino acids, NP_062389.1, GI: 9506757) was analyzed and the amino (Gal-12N-CRD, residues 1-167) and carboxy (Gal-12C-CRD, residues 168-314) CRDs were located. The construction for Gal-12N was based on the templates from Gal-9N structures (ID: 2D6N; 2D6M; 2D6K; 2D6L; 2D6P) with 36% sequence identity, and Gal-4N structures (ID: 2DYC; 3I8T) with 35% sequence identity. Comparative models were designed with Modeller 9.12 software.[24-26] Five structural models were generated for Gal-12N- and Gal-12C-CRDs, and selection of the best one was based on Molpdfs score (*Modeller Objective Function*). For Gal-12C, the following structures were used as templates: Gal-4C (ID: 1X50) with 20% sequence identity, Gal-8C (ID: 3OJB; 4GXL) with 18% sequence identity and Gal-9C (ID: 3NV1; 3NV4) with 18% sequence identity. All structural data were obtained from the RCSB-PDB database (Research Collaboratory for Structural Bioinformatics—Protein Data Bank—http://www.rcsb.org/).

2.2 | Hydrophobicity prediction

Hydrophobicity analysis of Gal-1, -4, -8, -9, and -12 and Perilipin was based on Kyte-Doolittle scale tool (http://gcat.davidson.edu/DGPB/kd/kytedoolittle.htm). The amino acid hydropathy scores are defined in http://gcat.davidson.edu/DGPB/kd/aminoacidscores.htm.

2.3 | Structural analysis and molecular modeling

For model structural analysis, VMD 1.9.1 (Visual Molecular Dynamics, Illinois, USA) software was employed.[27] Sequences were aligned and tertiary structures were overlaid. To describe the similarity between two structures, RMSD values were employed. In this work, C-Cα-N-O were considered as the backbone atoms.

2.4 | Molecular dynamics

Molecular dynamics (MD) studies were performed with Amber12 computational simulation package.[28] In all cases, Gal-12 structures were solvated with explicit three-site point charge modeled (TIP3P) water molecules in an octahedral box, localizing the box limits 10 Å away from the protein surface. MD simulations were performed at 1 atm and 300 K, maintained with the Berendsen barostat and thermostat,[29,30] using periodic boundary conditions and Ewald sums (grid spacing of 1 Å) for treating long-range electrostatic interactions with a 10 Å cut-off for computing direct interactions. The SHAKE algorithm was applied to all hydrogen-containing bonds, allowing employment of a 2 fs time step for the integration of Newton's equations. Amber ff99SB force field parameters[31] were used for all residues. The equilibration protocol involved a minimization of the initial structure, followed by 400 ps constant volume MD run heating the system slowly to 300 K. Finally, 0.8 ns MD run at constant pressure was performed to achieve proper density. MD runs of 50 ns for the model structures alone and for the Gal-12N complex with lactose (Lac), 3-fucosyllactose (3-FL), and 3′-sialyllactose (3′-SL) were performed. Frames were saved at 1 ps intervals. MD results were visualized with VMD software 1.9.1.[27]

2.5 | Ligand docking calculations

The structures of the modeled N-terminal and C-terminal domains of mGal-12 were edited for docking calculations using AutoDock Tools 1.5.6 software: polar hydrogens and partial charges were added explicitly, whereas the program

automatically adds other hydrogens. 3D carbohydrate structures of Lac, 2′-fucosyllactose (2′-FL), 3-FL, 2′,3-difucosyllactose (DFL), 3′-SL, 6′-sialyllactose (6′-SL), Lewis^X (LeX), and 3′-sialyl-3-fucosyllactose (SFL) were obtained from Glycam Carbohydrate Builder (glycam.org). Ligand structures were optimized with Avogadro 2.0.7 software.[32] The modeled structures of N- and C-terminal Gal-12 were used as models for the docking procedure with AutoDock Vina 1.2 software.[33] The docking protocol was initially set to rigid condition with a size of the dock grid of 16 × 16 × 16 Å, which encompasses the binding site for the carbohydrate ligands. Exhaustiveness was initially set to 10 with all other parameters set on default values, then was increased to 100 for final dockings. The top-ranked complexes, sorted by binding energy values, were visually inspected for good stereochemical geometry and docking. For visualization, docking poses generated by AutoDock Vina were directly loaded into PyMol (http://www.pymol.org) through PyMOL Autodock/Vina Plugin.[34] Images of the modeled receptor-ligand complexes were produced by PyMol and VMD 1.9.1 softwares.[27]

2.6 | Gene cloning

The coding sequence of full-length mGal-12 (Gene ID: 56072, SeqRNA ID: NM_019516) was cloned into pET28a plasmid (Novagen, 69864-3, Darmstadt, Germany) using the forward primer 5′-CATATGTCAACTGACGAACACC-3′ and the backward primer 5′-GGATCC TTAGCAGTGGACACAGTA GAGG-3′. The mGal-12 ORF was incorporated directionally with *NdeI* and *BamHI* restriction enzymes using the N-terminal 6xHis-tag. Cloning was confirmed by sequencing using primers as follows: T7 promoter (5′-TAATACGACTCAC TATAGGG-3′), reverse primer P2 (T7 terminator—5′-GCTA GTTATTGCTCAGCGG-3′) (Unidad de Secuenciación, Departamento de Ecología, Genética y Evolución, Facultad de Ciencias Exactas y Naturales, Universidad de Buenos Aires).

2.7 | Galectin-12 expression, purification, and identification

LB medium (1 l) containing 40 μg/mL kanamycin was inoculated with 10 mL of an overnight culture of Rosetta2 (DE3) pLysS *E. coli* cells (Novagen, Darmstadt, Germany) harboring the *pET28a-mGal-12* plasmid, and grown aerobically (37°C, 200 rpm) to $A_{600} = 0.4$. Gal-12 expression was then induced by the addition of isopropyl β-D-thiogalactoside (IPTG; 0.5 mM) and the incubation time was prolonged for 6 hours. Cells were harvested by centrifugation at 6000 *g* for 20 minutes, at 4°C and lysed by sonication with Buffer A (100 mM HEPES, 50 mM NaCl pH 6.1 containing 8 mM β-mercaptoethanol) supplemented with 0.5% DOC, lysozyme (4 mg/mL), DNAse 0.5 U/mL (Benzonase endonuclease), and protease inhibitors, 25 μM TLCK (tosyl-*L*-lysyl-chloromethane hydrochloride) and 0.5 mM PMSF (phenylmethylsulfonyl fluoride). Cells were lysed using an ultrasonicator and the insoluble fraction was removed by centrifugation (10 000 *g*, 4 °C, 30 minutes). The soluble fraction was dialyzed in Buffer A and then loaded to a Q-Sepharose column (GE Healthcare, Chicago, USA), previously equilibrated in Buffer A. The flow-through fractions containing Gal-12 were further purified by a carboxymethyl Sepharose (CM Sepharose, GE Healthcare Life Sciences, Chicago USA) cationic exchange resin with increasing NaCl concentration.

Gal-12 was eluted from CM Sepharose with 200 mM NaCl and those fractions were concentrated and dialyzed against Buffer A using a Vivaspin 20 concentrator (cutoff 30 000 MWCO, Sartorius, Göttingen, Germany), attaining a purification yield of 5 mg/l. Endotoxin-free recombinant Gal-12 was obtained by purification on a Detoxigel column (Thermo Fischer Scientific, Waltham, MA, USA) and stored at 2.5 mg/mL at −20°C in Buffer A supplemented with 20% glycerol. In these conditions, Gal-12 retained its activity for at least 4 months. Samples stored at 4°C lost their activity after 5-week storage. Protein content was monitored by Coomassie Plus protein assay reagent (Thermo Scientific, Waltham, MA, USA). Protein concentration during purification was determined by standard BCA Protein Assay (Thermo Fisher Scientific, Waltham, MA, USA) and NanoDrop 2000 UV-Vis spectrophotometer quantification (Thermo Fisher Scientific, Waltham, MA, USA). Recombinant Gal-12 was identified by SDS-PAGE (12%) and blotted onto nitrocellulose membranes (GE Healthcare, Chicago, IL, USA). Protein bands were identified using a rabbit anti-Gal-12 polyclonal antibody (clone H-166, Santa Cruz Biotechnology, Dallas, TX, USA, 1:700) or an in-house-generated rat anti-Gal-12 polyclonal antibody (Long-Evans rats, 1:1000 dilution). Then, proteins were detected using mouse anti-His-Tag monoclonal antibody (clone 4A12E4, Thermo Fisher Scientific, Life Technologies, Waltham, MA, USA, 1:500 dilution), mouse anti-β-actin antibody (C4, Santa Cruz Biotechnology, Dallas, TX, USA, 1:750 dilution) and the corresponding horseradish-peroxidase (HRP)-conjugated secondary antibodies. Immunoreactive protein bands were detected by chemoluminiscence (Pierce ECL Plus Western Blotting Substrate, Thermo Fisher Scientific, Waltham, MA, USA).

2.8 | Protein identification by mass spectrometry

Purified Gal-12 was loaded onto a 12% SDS-PAGE, stained with colloidal Coomassie Brilliant Blue G-250 and identified by mass peptide fingerprinting (CEQUIBIEM, Departamento

de Química Biológica, Facultad de Ciencias Exactas y Naturales, Universidad de Buenos Aires, Argentina). Peptide fragmentation data were matched against a protein database using MASCOT search engine (Matrix Science Inc., Boston, MA, USA).

2.9 | Anti-Gal-12 antibodies

The recombinant murine Gal-12 protein band was cut from a nitrocellulose membrane, homogenized, and mixed with incomplete Freund's adjuvant (1 mL). The emulsion was administered to four male 10- to 12-week-old Long Evans rats (250 µL per rat, s.c.), previously anesthetized with ketamine (25 mg/kg) and xylazine (1.5 mg/kg), and administration was repeated after 15 days. At day 30, 10 mL of blood was obtained by cardiac puncture from animals anesthetized with ketamine (50 mg/kg) and xylazine (3 mg/kg). Serum was filtered, diluted with PBS (1:10), and tittered against recombinant Gal-12 and used in further assays in a range from 1:1000 to 1:10 000 final dilution.

2.10 | Hemagglutination assay and hemagglutination inhibition assay

Hemagglutination assays (HAs) were performed as previously described.[35] Briefly, rabbit red blood cells (RBC) were trypsinized and fixed with glutaraldehyde 1% w/v, and stored at 4°C until use. The assay was performed in 96-well microplates (U-bottom) with sequential dilutions of mGal-12 in PBS buffer. Trypsinized RBC in PBS buffer was added, gently mixed by pipetting, and incubated 2-3 hours at 4°C. Asialofetuin (ASF), obtained by mild acid hydrolysis of fetuin (Sigma-Aldrich, St. Louis, MO, USA) in 2N acetic acid, 2 hours, 80°C, was used as potential Gal-12 ligand.

2.11 | Solid phase assays

The assay was adapted from Rapoport et al.[36] Briefly, 96-well plates (flat-bottom) were coated with 10 µg/mL ASF in sodium carbonate buffer (pH 9.6) and incubated overnight at 4°C. Then, wells were washed three times with 100 µL/well PBS-Tween 0.05% (w/v) and blocked with 100 µL/well PBS-BSA 2% (1 hours, RT) in a humid chamber. Meanwhile, equal volumes of Gal-12 (30 µg/mL) in PBS-BSA 0.3% buffer were pre-incubated with the corresponding inhibitors in serial dilutions (2 hours, 37°C). All oligosaccharides tested were purchased from Elicityl (Grenoble, France), except lactose that was purchased from Sigma Aldrich, St. Louis, MO, USA. Lactose (Lac), 6′-sialyllactose (6′-SL), 2′-fucosyllactose (2′-FL), 3-fucosyllactose (3-FL), 2′,3-difucosyllactose (DFL), Lewis^X (Le^X) trisaccharide, and 3′-sialyl-3-fucosyllactose (SFL) were evaluated as potential Gal-12 competing ligands in the presence of immobilized ASF (2 hours, 37°C). After washing, Gal-12 was detected using a 1:500 dilution of anti-mGal-12 rabbit antibody (H-166, Santa Cruz Biotechnology, Dallas, TX, USA) in PBS-BSA 0.3 % w/v (1 hour, RT) and an anti-rabbit secondary antibody conjugate coupled to HRP (1 hour, RT, in PBS-BSA 0.3 % w/v). Finally, tetramethylbenzidine (TMB) (1:3000 dilution, Vector Labs, Burlingame, CA, USA) and 30% v/v H_2O_2 (1:5000 dilution) in cold citrate buffer (pH 5.5) were used to quantify ASF-bound Gal-12. The reaction was stopped with 25 µL 2N H_2SO_4 and the absorbance was measured at 450 nm using a plate spectrophotometer (Multiskan Ex, Thermo Fisher Scientific, Waltham, MA, USA).

2.12 | Isothermal titration calorimetry assays

Glycans used in solid phase assays (SPAs) were evaluated as inhibitors of Gal-12 by isothermal titration calorimetry (ITC). A NanoITC instrument (TA Instruments, New Castle, DE, USA) was used for titrations at 298 K. Syringe, cell concentrations and molar ratios, injection volumes, and time intervals between injections varied to obtain sufficient heat production per injection to allow good peak integration and enough time between injections to allow a return to equilibrium. A typical titration involved 20 injections at 3 minutes intervals of 2.5 µL aliquots of 2.5 mM ligand solution into the sample cell (200 µL) containing Gal-12 (50 µM). The syringe and cell solutions were prepared by dissolving glycan ligands and Gal-12 in Buffer A at 298 K. The titration cell was continuously stirred at 300 rpm. Heats of dilution of the glycan ligands in Buffer A were subtracted from the titration data. Fitting was performed using NanoAnalyze software to determine the binding stoichiometry (n), dissociation constant (K_d), and the enthalpy change (ΔH).

2.13 | Cell culture and adipocyte differentiation assays

Pre-adipocytes 3T3-L1 cells (ATCC CL-173, Manassas, VA, USA) were grown in DMEM medium (GIBCO) containing 10% FBS (GIBCO, Life Technologies, Waltham, MA, USA) and supplemented with 100 U/mL penicillin-streptomycin and 0.25 µg/mL Fungizone Antimycotic (Gibco Antibiotic-Antimycotic, Life Technologies, Waltham, MA, USA) at 37°C in 5% CO_2. To trigger adipocyte differentiation, 3T3-L1 cells were plated at a 1×10^6 cells per well in p60 plates and cultured for 2 days.[37] Differentiation was induced (day 0) by the addition of 0.5 mM isobutyl-methyl-xanthine (IBMX),

1 μM dexamethasone, and 1 U/mL human insulin isophane (NPH) for 7 days, replacing special media every 2 days. The induction medium was removed, and cells were supplemented with DMEM plus 10% FBS and 1 U/mL human insulin isophane (NPH) during 5 additional days. HUVEC (kindly provided by Dr. Mirta Schattner; Experimental Thrombosis Lab, Academia Nacional de Medicina, Buenos Aires) were maintained in RPMI medium (Gibco) supplemented with 20% fetal calf serum (FCS), bFGF (10 ng/mL), VEGF-A (20 ng/mL) (all purchased from R&D, Minneapolis, MN, USA) and used between passages 2 and 5.

2.14 | Induction of hypoxia

3T3-L1 cells differentiated to adipocytes were cultured in 24-well plates, placed in a modular incubator chamber (Billups-Rothenberg, San Diego, CA, USA) and flushed at 2 psi for 10 minutes with a mixture of 1% O_2, 5% CO_2, and 94% N_2. The chamber was sealed and placed in a 37°C incubator for 18 hours. Controls of normoxia were placed in the same incubator at 20% O_2.

2.15 | Glycophenotyping of endothelial cells

HUVEC were incubated with biotinylated lectins, during 30 minutes at RT in lectin buffer (150 mM NaCl, 10 mM HEPES, 1% BSA) as follows: *Ulex europaeus* Agglutinin I (UEA-1, 5 μg/mL), L-*Phaseolus vulgaris* (L-PHA, 2 μg/mL), *Aleuria aurantia* lectin (AAL, 2 μg/mL), *Sambucus nigra* lectin (SNA, 2 μg/mL), *Maackia amurensis* lectin II (MAA, 5 μg/mL), Concanavalin A (Con A, 2 μg/mL), and *Lycopersicon esculentum* lectin (LEL, 2 μg/mL). After washing, cells were incubated with Phycoerythrin (PE)-conjugated streptavidin (Sigma) during 45 minutes at RT and analyzed by flow cytometry (Accury C6 plus, BD). All lectins were purchased from Vector Labs, Burlingame, CA, USA. Additionally, and to identify specific sialyl Lewis-X structures, cells were incubated with Alexa Fluor 488 labeled anti-CD15s antibody (1/200 clone cslex1, BD) during 45 minutes on ice and analyzed as described above. Analysis was performed with FlowJo V10.7 (FlowJo LLC) and Prism 6 (GraphPad) software.

2.16 | Mice

Lgals12$^{-/-}$ mice (C57BL/6) were generated as described.[22] Mice (*Lgals12*$^{-/-}$ and WT) were bred at the animal facility of the Instituto de Biología y Medicina Experimental (IBYME) according to National Institutes of Health (NIH, USA) guidelines. All experimental procedures were reviewed and approved by the Institutional Animal Care and Use Committee (Instituto de Biología y Medicina Experimental, IBYME, Buenos Aires, Argentina).

2.17 | Angiogenesis assays

The formation of capillary-like tubular structures was assessed in Geltrex-coated plates (Thermo-Scientific, Waltham, MA, USA) essentially as described.[38] In brief, HUVEC (1.5×10^4 cells/mL) were exposed to recombinant Gal-12 (0.1 to 3 mM) with or without Lac (2 mM) or 3-FL (400 μM) and plated on Geltrex-coated 96-well plates at 37°C for 16 hours. Capillary-like tubular structures were recorded by counting the number of tubules (closed areas) per well in a phase-contrast microscope (Nikon Eclipse TE300).

For migration assays, HUVEC (4×10^4 /cm^2) were resuspended in RPMI medium supplemented with 1% FCS. Cells were placed into the top chamber of the 8 μm insert while the bottom well was filled with recombinant Gal-12 in the absence or presence of Lac (30 mM) or 3-FL (400 μM). After 24 hours, cells were fixed and stained with 0.05 % crystal violet (Sigma Aldrich, St. Louis, MO, USA) and analyzed in an inverted microscope. For each insert, four images were collected and cells were counted with the ImageJ software v2.0.0 (Fiji Software).

2.18 | Staining and imaging

For adipocyte staining, cells were grown on glass coverslips, washed with PBS and fixed with 4% paraformaldehyde (PFA) and 20% sucrose in PBS (25 minutes, RT). After blocking with 0.2 M glycine (45 minutes, RT), coverslips were incubated ON (4°C) with anti-Gal-12 rat serum (1:10 000), and/or anti-perilipin-1 (1:200, Cell signaling, Danvers, MA, USA). Then, coverslips were washed with PBS and incubated during 60 minutes at RT with anti-rabbit IgG Alexa Fluor 647 and anti-rat IgG Alexa Fluor 555, and/or Bodipy 493/503 dye (Invitrogen, Thermo Fisher Scientific, Waltham, MA, USA). Finally, they were washed and mounted with Vectra-Oil and Hoechst 33342 as counterstain.

Non-specific staining of in house anti-Gal-12 rat serum was ruled out by incubation with pre-immune rat serum (1:10 000) and then anti-rat Alexa Fluor 555 and Bodipy. To analyze non-specific interactions between secondary antibodies, coverslips previously incubated with primary antibody rabbit anti-Perilipin-1 in the absence of anti-Gal-12 antibody were incubated with anti-rabbit Alexa Fluor 647 and anti-rat Alexa Fluor 555. Samples were visualized on a FV1000 confocal microscope (Olympus, Shinjuku, Tokio, Japan) using a 60× UPLSAPO objective with a numerical aperture of 1.35. Secondary antibodies for Gal-12 and Perilipin-1, anti-rat IgG Alexa Fluor 555, and anti-rabbit IgG Alexa Fluor 647 were

excited using 543 nm He-Ne laser and 635 nm diode laser, respectively, and the emitted fluorescence was detected in the 560-625 nm and 655-755 nm range. To detect LDs, Bodipy 493/503 was excited using the 488 nm line of the Argon laser and the emitted fluorescence was detected in the 500-530 nm. To avoid crosstalk between fluorescence signals, images were recorded line by line in a sequential order. Under these conditions, employing single stained samples, no spectral overlap was detected. Moreover, autofluorescence was monitored in cells with no staining and was found to be negligible. Intensity profiles for each channel were calculated, averaging 10 consecutive pixels (approximated 0.5 μm), along the radial direction of LDs and then normalized to the maximum and minimum fluorescence intensity. Images were analyzed using Fiji software (ImageJ, NIH).[39]

For vasculature networks in vivo visualization, mice were anesthetized and intravenously injected with DyLight-594 labeled *Lycopersicon esculentum* lectin (LEL, Vector Labs, Burlingame, CA, USA) prior cardiac-perfusion with PBS. Tissues were removed, fixed with 4% PFA 20% sucrose for 24 hours, and embedded in optimal cutting temperature (OCT) compound. Sections (70 μm) were counterstaining using Hoechst 33342 (Sigma Aldrich, St. Louis, MO, USA) and mounted in Vectra-Oil. Samples were visualized on FV10i confocal microscope (Olympus, Shinjuku, Tokyo, Japan) and analyzed using Fiji 1.0 software (ImageJ, NIH).

2.19 | Real-time quantitative PCR

Total RNA from 3T3-L1 cells was purified using TRIzol reagent (Life Technologies, Thermo Fisher Scientific, Waltham, MA, USA) and DNAse (Promega, Madison, WI, USA). cDNA was synthesized using SuperScript II™ (Invitrogen, Life Technologies, Waltham, MA, USA) according to manufacturer's instructions. mRNA was measured by RT-PCR using *Taq* polymerase (Invitrogen, Life Technologies, Waltham, MA, USA) and relative gene expression was analyzed using SYBR Green PCR Master Mix (Applied Biosystems, Thermo Fisher Scientific, Waltham, MA, USA) and ABI PRISM 7500 Sequence Detection Software (Applied Biosystems, Thermo Fisher Scientific, Waltham, MA, USA). Results were normalized using β-actin as control. Primers used were as follows: mGal-12 forward, 5-AACTGACGAACACCTGGACC-3; mGal-12 reverse, 5-TGCCATAAGGAATCACCGGG-3; β-actin forward, 5-AGCTGCGTTTTACACCCT-3; β-actin reverse 5-AAGCCATGCCAATGTTGTCT-3.

2.20 | Statistical analysis

Prism software (GraphPad) was used for statistical analysis. Student's *t* test was used for unpaired data. Two-way ANOVA and Dunnett's or Tukey post-tests were used for multiple comparisons. *P* values of .05 or less were considered significant.

3 | RESULTS

3.1 | *In silico* analysis

To identify the structural determinants of Gal-12 function, we first performed *in silico* analysis of this protein. mGal-12 is a tandem-repeat type galectin with a molecular weight of 35.5 kDa and a high isoelectric point (pI 8.9), which presents two distinct CRDs: its N-terminal CRD is homologous to other members of the galectin family, displaying five of the seven amino acid residues essential for Lac binding (Arg^{77}, Asn^{88}, Trp^{95}, Glu^{98}, and Arg^{100}). However, the N-terminal CRD does not present the His and Asn residues highly conserved in the S4 strand (Figure 1), essential for stabilizing lactose binding. These residues are replaced by Arg^{72} and Ser^{74}, respectively. Conversely, Gal-12 C-terminal CRD exhibits considerable divergence and, in opposition to other tandem-repeat type galectins, only presents the highly conserved Trp^{257} residue responsible for stacking interactions with the hydrophobic face of galactose moieties[40] (Figure 1). When compared to other tandem-repeat type galectins, Gal-12 exhibits a highly hydrophobic profile (Figure S1A), similar to other proteins found in LD such as perilipin-1, in accordance with its expression in adipocyte LDs.[18,22]

3.2 | Galectin-12 cloning, expression, and purification

To generate full-length Gal-12 with a cleavable N-terminal histidine (6xHis) tag for biochemical and functional studies, mGal-12 ORF (NCBI Ref Seq: NM_019516.5, 945 bp, from 464 to 1408 bp) was cloned into a pET-28a plasmid vector using the *NdeI/BamHI* cleavage sites (*pET28a-mGal-12* construct). First attempts to express untagged Gal-12 were unsuccessful, due to the fact that Gal-12 was obtained in the insoluble fraction and could not be re-solubilized (data not shown). Moreover, when construct *pET28a-mGal-12* was transformed into *E. coli* BL21 (DE3) cells, Gal-12 was still obtained as part of the insoluble fraction. These results prompted us to use *Escherichia coli* Rosetta 2 (DE3) cells with *pET28a-mGal-12*, since this strain supplies extra tRNAs for translation of eukaryotic proteins. We obtained Gal-12 in the soluble fraction after lysis. Since a considerable proportion of recombinant Gal-12 was still obtained in the insoluble fraction and resolubilization with urea was not successful, we evaluated a potential association of Gal-12 with the membrane pellet by means of its hydrophobicity. Addition of

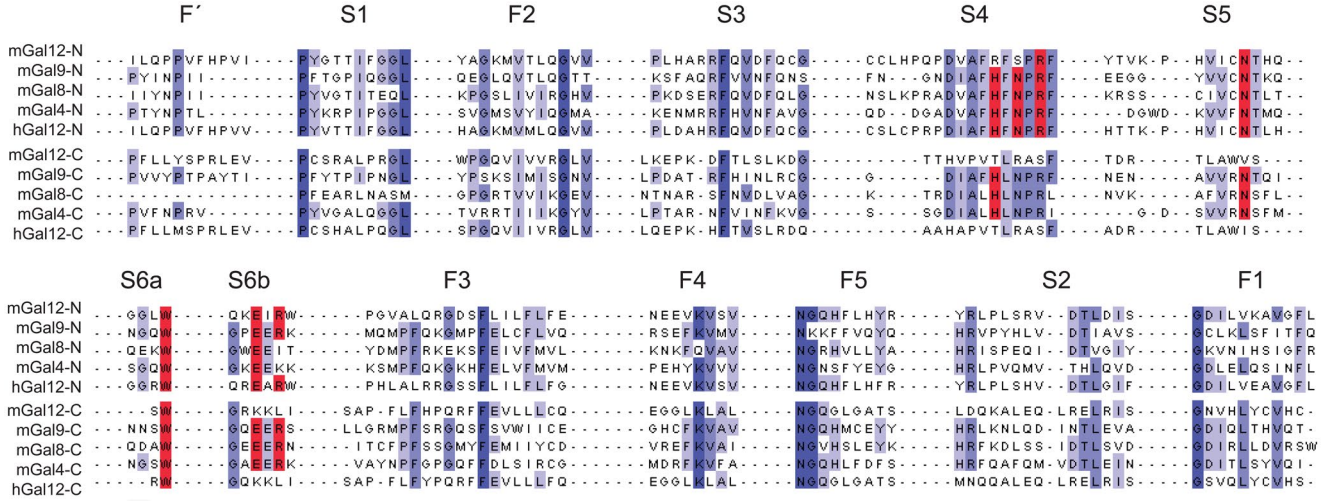

FIGURE 1 Sequence alignment of *Mus musculus* tandem-repeat type galectins (Gal-4, -8, -9, and -12) and hGal-12. Sequences were aligned using Jalview.[75] Each carbohydrate recognition domain (CRD) consist of 135-165 amino acids, arranged on two antiparallel β-sheets, each composed of six (F′-F5 and S1-S6) β-strands. Tandem-repeat type galectins are composed of two non-identical CRDs joined by a hinge region. The highly conserved residues in the galectin family, essential for protein-carbohydrate interactions, are highlighted in red. Identical residues are highlighted in blue and similar residues in light blue

glycerol 5% or different detergents to the lysis buffer (100 mM HEPES, 50 mM NaCl pH 6.1, 8 mM β-mercaptoethanol, Buffer A) proved to be unsuccessful. However, 0.5% sodium deoxycholate (DOC) provided an important improvement in generating soluble protein. Thus, Buffer A supplemented with 0.5% DOC was used for further Gal-12 purification. Surprisingly, both His-tag-Gal-12 purification by Ni-NTA beads and lactosyl-sepharose affinity chromatography (the latter previously described for hGal-12 purification[20] were ineffective. Thus, we optimized a two-step chromatographic protocol with a serial anionic/cationic exchange, through which recombinant Gal-12 was successfully obtained with a total yield of 5 mg/L culture (Figure 2A,B), and positively identified by peptide fingerprinting (Figure S1B). Consistent with its hydrophobic nature, even after purification, Gal-12 was highly prone to aggregation at concentrations higher than 1 mg/mL.

3.3 | Recombinant Gal-12 displays hemagglutinating activity

To characterize the lectin activity of purified Gal-12, we evaluated its glycan-dependent hemagglutinating function as described.[35] Recombinant Gal-12 was able to agglutinate trypsin-fixed rabbit erythrocytes at concentrations of 1 μg/mL or higher (Figure 2C). In contrast to other galectins[41] and consistent with its lack of interaction with lactosyl-Sepharose, the hemagglutinating activity of Gal-12 could not be inhibited by lactose (Figure 2D). As lectins usually present low affinities toward free oligosaccharides when compared to complex glycoproteins presenting multivalency and high ligand density,[13] we decided to test ASF, a well-known ligand for other galectins, as a potential assay inhibitor. Notably, this glycoprotein successfully inhibited Gal-12-induced hemagglutinating activity (Figure 2D), setting the bases for the development of SPA.

3.4 | Recombinant Gal-12 shows preference for 3-fucosylated moieties in solid-phase assays

Gal-12 binding to ASF-coated surfaces was detected in solid-phase assays using a rabbit anti-Gal-12 polyclonal antibody. Several neutral, sialylated, and fucosylated oligosaccharides were tested as competitive inhibitors of ASF-Gal-12 interactions (Table 1, Figure 2E,F), confirming that lactose is a poor Gal-12 ligand ($IC_{50} > 10$ mM). In addition, 3′-SL presented an IC_{50} of 5 mM, evidencing that 3′-sialylation increases Gal-12 binding, whereas α2,6-sialylation does not improve Gal-12 binding to lactose, as observed for other galectins.[42] Notably, fucosylation was found to be a key molecular feature for Gal-12 binding: Lewis X (Le^X) and 3′-fucosyllactose (3′-FL) showed the best inhibitory results ($IC_{50} = 3 \pm 1.0$ and 0.3 ± 0.1 mM, respectively; Figure 2E and Table 1). However, 2′,3-difucosyllactose (2′,3-DFL) presented an IC_{50} similar to 3-FL (Figure 2E), demonstrating that α1,2-fucosylation on the galactose moiety does not affect Gal-12 binding.

Further evaluation of the fucosylated Gal-12 ligands by Isothermal Titration Calorimetry (ITC) revealed the thermodynamic dissociation constant (K_d) values for each structure (Table 2). In accordance with the results previously obtained, Gal-12 showed again low affinity toward lactose ($K_d = 661 \pm 65$ μM). Furthermore, sialylated and

2′-fucosylated glycans presented lower affinity compared to their 3-fucosylated counterparts, as 3-FL and Le^X oligosaccharides were preferred Gal-12 ligands (Table 2). The increased affinity provided by the single addition of the fucose moiety in the glucose 3-OH of lactose is shown in Figure 2G,H. Taken together, these results indicate that, differently from other members of the galectin family,[43] Gal-12 has unique binding preferences toward 3-fucosylated oligosaccharides.

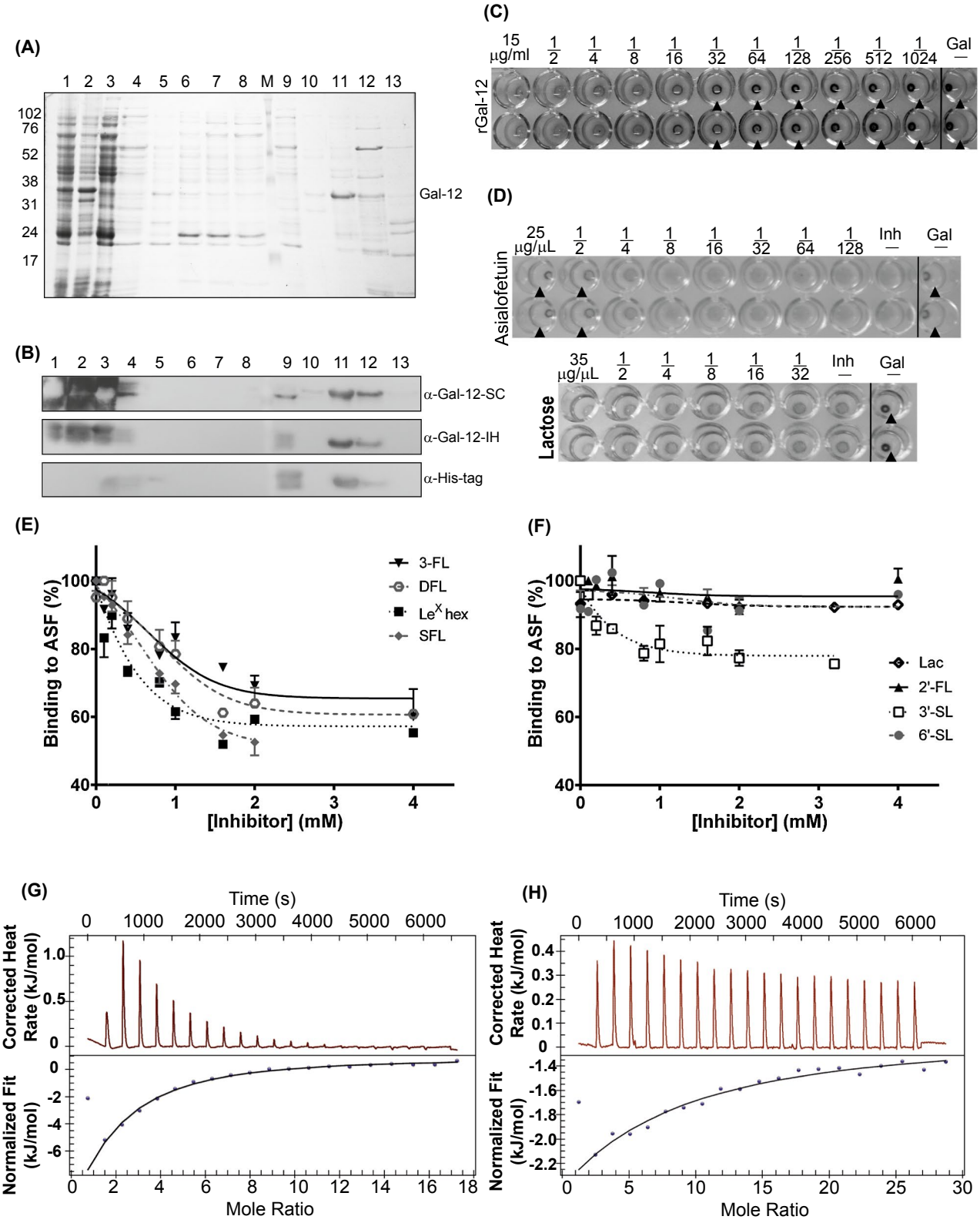

FIGURE 2 Expression, purification, and biochemical characterization of mGal-12. A, Purification of recombinant Gal-12 by serial anionic/cationic chromatography. Fractions were run in 12% SDS-PAGE and total proteins were stained with Coomassie blue. Lane 1, crude soluble extract; Lane 2, soluble extract filtered with 45 μm nylon membrane; Lane 3, insoluble extract; Lane 4, Q-Sepharose flowthrough (buffer A); Lanes 5, 6, 7, and 8 correspond to Q-Sepharose elution fractions (buffer A) with increasing NaCl concentration (100, 150, 200, and 250 mM, respectively); Lane 9, CM-Sepharose flowthrough (buffer A); Lanes 10, 11, 12, and 13 correspond to CM-Sepharose elution fractions (buffer A) with increasing NaCl concentration (100, 200, 250, and 300 mM, respectively). B, Western blot of recombinant Gal-12 purified by serial anionic/cationic chromatography. Gel was prepared and run using the same conditions as in panel A for commercial anti-Gal-12 from Santa Cruz Biotechnol (α-Gal-12-SC) rabbit polyclonal antibody, in-house-generated anti-Gal-12 (α-Gal-12-IH) rat polyclonal antibody and anti-HisTag antibody. C, Hemagglutinating activity of mGal-12. Serial dilutions of recombinant Gal-12 were tested on trypsin-treated rabbit erythrocytes. Arrowheads indicate no agglutination of erythrocytes. Lysis buffer A was used as negative control and human recombinant Gal-1 was used as a positive control (data not shown). D, Inhibition of Gal-12 hemagglutinating activity. ASF and lactose were tested as Gal-12 competitive ligands in serial dilutions. Gal-12 concentration was 3 μg/mL. E,F, SPAs showing Gal-12 affinity for different oligosaccharides. ASF was immobilized as a Gal-12 ligand and competitive assays with serial dilutions of 3-fucosylated oligosaccharides (E) and lactose, sialylated and 2′-fucosylated glycans (F) were performed. Gal-12 binding to ASF was detected with rabbit anti-Gal-12 antibody. Results are representative of six independent experiments. G,H, Experimental calorimetric data associated with the isothermal titration at 298 K of (G) mGal-12 (50 μM) with 3-FL (2.5 mM) and (H) mGal-12 (30 μM) with lactose (2.5 mM). Abbreviations: ASF, asialofetuin: Lac, lactose; 6′-SL, 6′-sialyllactose; 2′-FL, 2′-fucosyllactose; 3-FL, 3-fucosyllactose; DFL, 2′,3-difucosyllactose; Le^X, Lewis X trisaccharide and SFL, 3′-sialyl-3-fucosyllactose

TABLE 1 Half maximal inhibitory concentration (IC_{50}) for the tested oligosaccharides by solid phase assays. The IC_{50} values shown correspond to the mean of three independent determinations. Lac, lactose; 2′-FL, 2′-fucosyllactose; 3-FL, 3-fucosyllactose; DFL, 2′,3-difucosyllactose; Le^X, lewis X oligosaccharide (3-fucosyl *N*-acetyllactosamine); SFL, 3′-sialyl-3-fucosyllactose; 3′-SL, 3′-sialyllactose; 6′-SL, 6′-sialyllactose

Compound	IC_{50} (mM)
Lac	>10
2′-FL	7.0 ± 1.0
3-FL	3.0 ± 1.0
DFL	4.0 ± 1.0
Le^X	0.3 ± 0.1
SFL	2.0 ± 0.4
3′-SL	5.0 ± 1.0
6′-SL	>10

TABLE 2 Dissociation constant (K_d) values of the tested oligosaccharides toward Gal-12 obtained by isothermal titration calorimetry. The K_d values shown correspond to the mean of three independent determinations. Lac, lactose; 2′-FL, 2′-fucosyllactose; 3-FL, 3-fucosyllactose; DFL, 2′,3-difucosyllactose; Le^X, lewis X oligosaccharide (3-fucosyl *N*-acetyllactosamine); SFL, 3′-sialyl-3-fucosyllactose; 3′-SL, 3′-sialyllactose; 6′-SL, 6′-sialyllactose

Ligand	K_d (μM)
Lac	661 ± 65
2′-FL	792 ± 87
3-FL	54 ± 4
DFL	191 ± 21
Le^X	66 ± 9
SFL	151 ± 18
3′-SL	301 ± 28
6′-SL	889 ± 106

3.5 | Homology modeling of murine galectin-12 N- and C-terminal CRDs

To provide further insights into the atomistic determinants of Gal-12 interaction with fucosylated glycans, and considering that no crystal structure of Gal-12 has yet been reported, we generated mGal-12 N- and C-terminal domains structural models by comparative modeling based on other tandem-repeat galectins (Gal-4, Gal-8, and Gal-9) as reference frameworks. Furthermore, splitting the protein into the two CRDs allowed us to study each domain separately, as previously described for other tandem-repeat galectins.[44] Murine Gal-12N-CRD was constructed based on mGal-9N and mGal-4N crystal structures (Figure 3A), and since no crystallized structure is available for the C-terminal domain of any murine tandem-repeat galectin, hGal-4C, hGal-8C, and hGal-9C were used as templates for mGal-12C-CRD (Figure 3B). Despite the low similarity sequence, all models successfully presented a GA341 score of 1.00, suggesting that they are reasonable models. The best ones were selected with regard to the final molpdf scores calculated (Table S1), namely models 2 and 3 for the N- and C-terminal domains, respectively.

Our homology models for mGal-12N-CRD presented six β-strands in the S-sheet (S1-S6) and six β-strands in the F-sheet (F1-F5, plus F′; Figure 3A). The extra F strand (F′) is only present in tandem-repeat type galectins, such as Gal-8 and Gal-9 and does not directly affect binding of any potential ligand, since it is placed on the convex side of the overall structure. MD simulations showed a converged structural stability for both models (Figure S2). These structural models showed five different hydrophobic zones

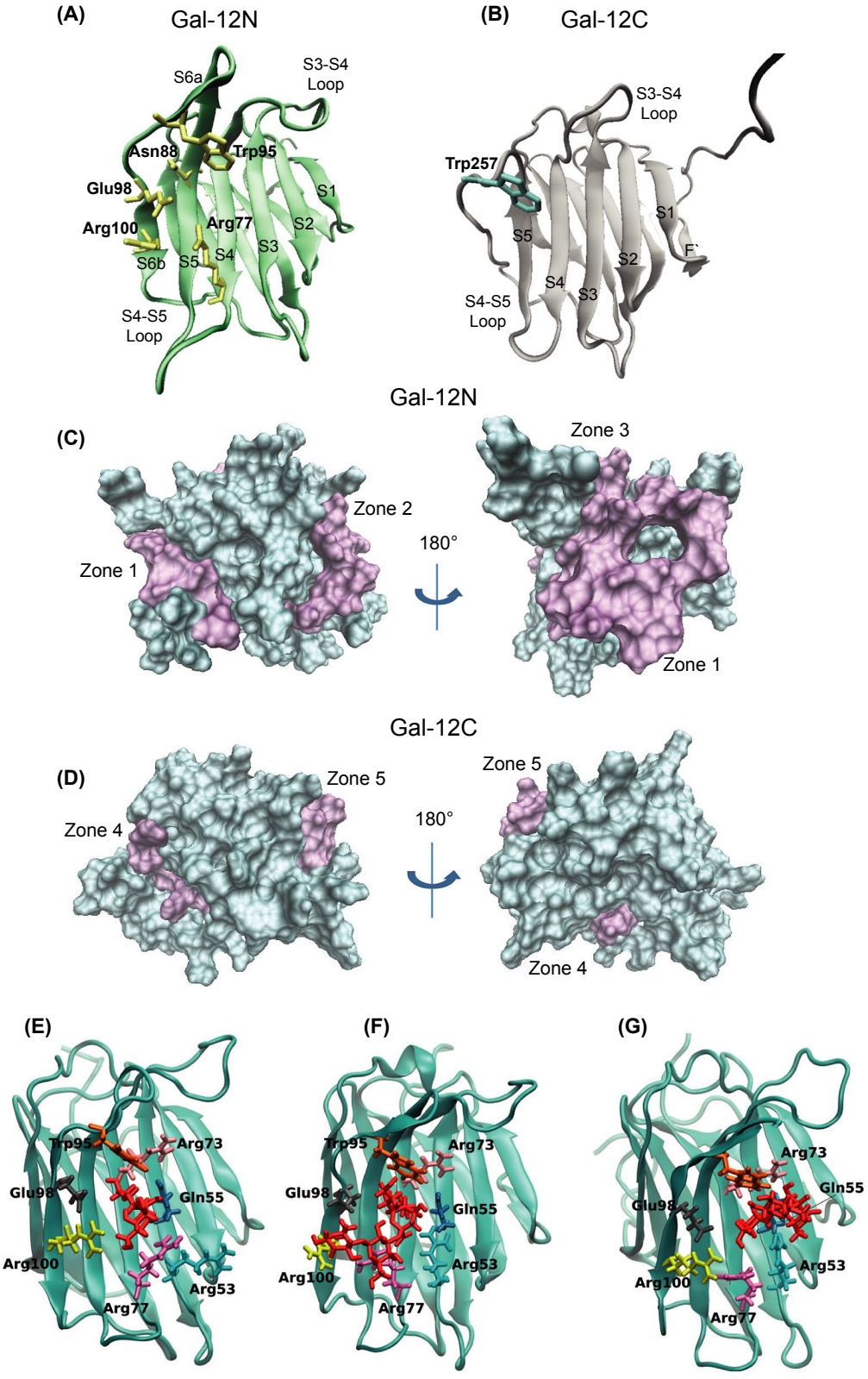

FIGURE 3 Homology models and molecular dynamics studies. Modeled structures of the A, N-terminal and B, C-terminal domains of Gal-12. Galectin structures are presented in new cartoon representation and essential conserved residues from the LBG are shown in licorice representation. Spatial distribution of hydrophobic zones according to the generated structural models for C, Gal-12N and D, Gal-12C. Zone 1 (residues 8-34, F′ strand); zone 2 (residues 98-106, S6b strand); zone 3 (residues 139-153, S2 strand); zone 4 (residues 190-198, S1 strand) and zone 5 (residues 250-258, S6a/S6b strands). Hydrophobic zones are colored in purple in surf representation. Models of interaction between Gal-12N and E, lactose, F, 3′-sialyllactose and G, 3-fucosyllactose were obtained by molecular dynamics. Gal-12 CRDs are shown in NewCartoon representation with key amino acid side chains in licorice and oligosaccharide ligands in red

in Gal-12 (Figure 3C,D): zone 1 (residues 8-34, comprising the F′ strand), zone 2 (residues 98-106, S6b strand), and zone 3 (residues 139-153, S2 strand) were present in the amino-terminal CRD (Figure 3C), while zone 4 (residues 190-198, S1 strand) and zone 5 (residues 250-258, S6a/S6b strands) corresponded to the C-terminal CRD (Figure 3D). While hydrophobic zones 2, 3, and 4 are disposed toward the core of the protein, zones 1 and 5 are more exposed toward the solvent.

3.6 | Docking and molecular dynamics of Gal-12 ligands

To analyze molecular interactions defining Gal-12-binding affinity evidenced by SPA and ITC, we used Gal-12N and Gal-12C structural models. Theoretical affinity score values for the interactions between Gal-12N and Gal-12C and the different tested oligosaccharides were calculated by molecular docking studies (Table 3). The theoretical binding preferences for Gal-12N, significantly higher than those observed for Gal-12C, were in agreement with the experimental results obtained with full-length Gal-12 by SPA and ITC (Figure 2E,F and Table 2). MD simulations of the Gal-12N structural model complexed with lactose, 3′-SL or 3-FL, showed that Arg^{73} is in close interaction with fucose O4 in 3-FL (Figure 3E-G), which could explain the binding preference of this lectin for 3-fucosylated glycans. Correlation plots between experimental and theoretical data are shown in Figure S2B.

3.7 | Gal-12 expression is modulated by hypoxia

To better understand the biological relevance of Gal-12 in AT, we evaluated Gal-12 expression during differentiation of 3T3-L1 cells into adipocytes, both by RT-PCR and Western blot. In accordance to previous reports,[18] Gal-12 expression progressively increased after stimulation with adipogenic hormones, reaching a peak at day 10 post-differentiation, both at mRNA and protein levels (Figure 4A,B). Given that local tissue hypoxia accompanies AT remodeling, we next evaluated whether this stimulus could trigger Gal-12 expression. We found increased Gal-12 expression when adipocytes were cultured under hypoxic conditions as evaluated both by RT-PCR (Figure 4C) and Western blot (Figure 4D). Thus, Gal-12 may be part of the hypoxia-regulated response triggered in adipocytes to overcome cellular stress.

For cellular localization, we used an in-house-generated anti-Gal-12 rat serum described in *Materials and Methods*. To characterize reactivity of this polyclonal anti-Gal-12 serum, we evaluated non-specific staining by treating samples with preimmune rat serum as control. These results showed no label within LDs, in comparison with samples incubated with rat anti-Gal-12 antibody (1:10000) (data not shown). Moreover, non-specific interactions between secondary antibodies were ruled out as no specific labeling of (a) anti-rat Alexa Fluor 555, (b) primary anti-Gal-12 antibody in the absence of rabbit anti-Perilipin-1 antibody and anti-rabbit Alexa Fluor 555 were observed (data not shown). Confocal microscopy showed that Gal-12 was predominantly located on large LDs with increased expression during cell differentiation (Figures 4E, S3). Moreover, these experiments provided evidence of a differential distribution pattern for Gal-12 and perilipin-1. While Gal-12 was mainly circumscribed to the inner LD region, and preferentially occupied LD space without fatty acids (as its immunoreactive signal did not colocalize with Bodipy), perilipin-1 was associated with the LD membrane (Figure 4E). Intensity profiles for each channel along the radial direction of LD (and then normalized to the maximum and minimum fluorescence intensity) showed contrasting positions between Gal-12, perilipin-1, and fatty acids (Figure 4F).

TABLE 3 Affinity scores values obtained by *in silico* docking of Gal-12N and Gal-12C structural models with selected oligosaccharides

	Affinity (kcal/mol)	
Ligand	**Gal-12N**	**Gal-12C**
Lac	−4.8	−3.6
2′-FL	−4.6	−3.7
3-FL	−6.0	−3.3
DFL	−5.8	−3.2
Le^X	−5.9	−3.4
FSL	−5.41	−3.5
3′-SL	−5.21	−3.8
6′-SL	−4.4	−3.1

3.8 | Gal-12 promotes angiogenesis through binding to 3-fucosylated glycans in endothelial cells

Since hypoxia-driven angiogenesis plays a key role in response to AT distress, and because Gal-12 is upregulated under this condition, we next investigated whether this lectin was involved in the control of endothelial cell biology. To address this issue, we first examined the glycosylation signature of HUVEC exposed to hypoxic (1% O_2, 18 hours) or normoxic conditions using a set of biotinylated lectins. Since Gal-12 preferentially binds to 3-fucosylated glycans (Figure 2E, Tables 1 and 2), we first evaluated binding of UEA-1 and AAL (lectins that recognize fucosylated residues). Interestingly, fucosylated glycans were found to be upregulated in HUVEC surface glycoconjugates under hypoxic conditions (Figure 5A). On the contrary, abundance of α2,3-sialylated moieties (as evaluated by MAA binding) and

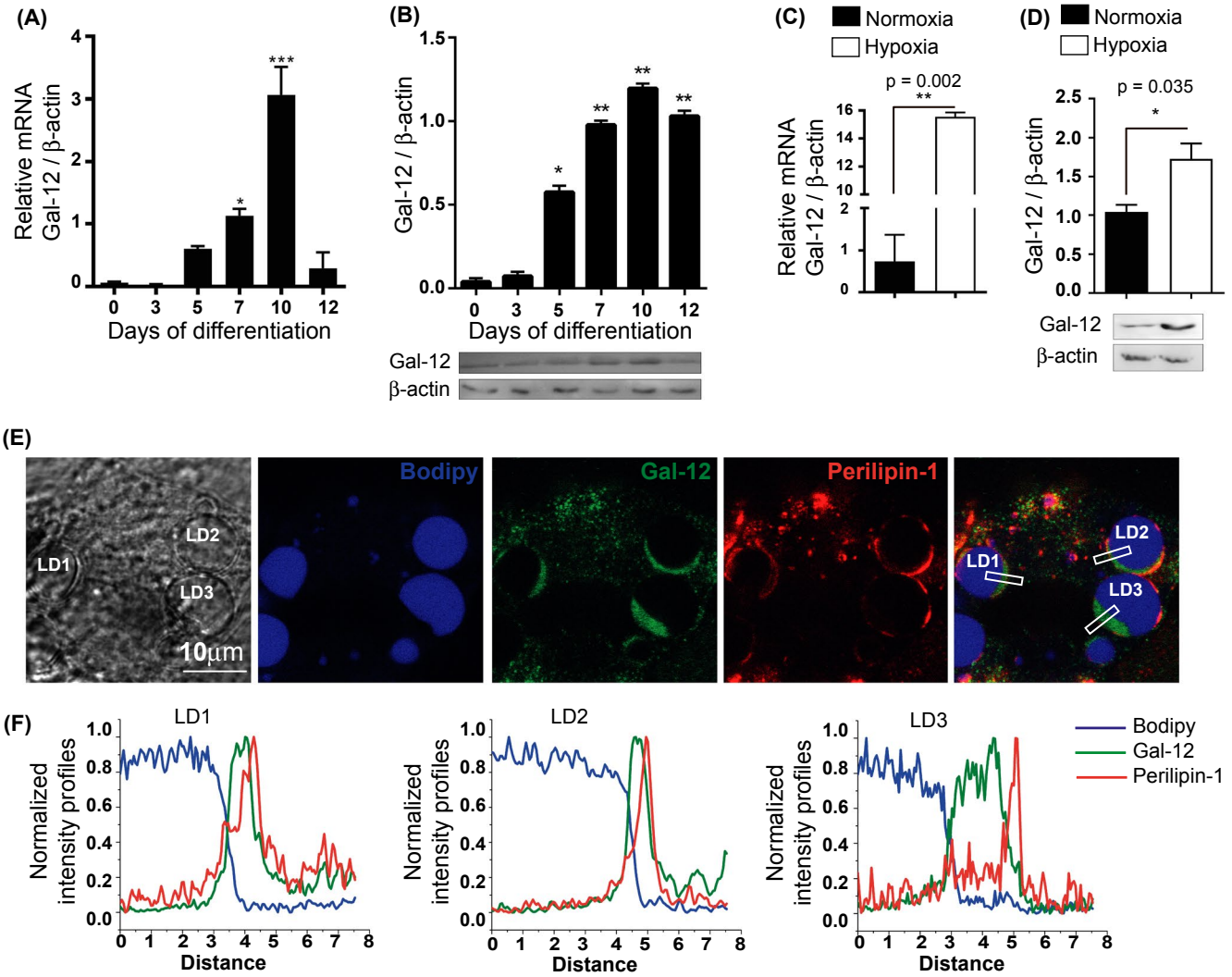

FIGURE 4 Expression of Gal-12 is modulated by hypoxia. Gal-12 expression in differentiating 3T3-L1 cells analyzed by A, RT-PCR and B, immunoblot assays. 3T3-L1 cells at day 6 of differentiation were grown under normoxic and hypoxic conditions for 18 hours and analyzed by C, RT-PCR and D, immunoblot assays. E, Representative adipocyte staining of neutral lipids (Bodipy), Gal-12, and Perilipin-1 at day 12 of differentiation. Scale bar: 10 μm. F, Normalized intensity profiles along the selected areas (E) for neutral lipids (blue), Gal-12 (green), and Perilipin-1 (red). In all cases, the inside of lipid droplets is shown at the left. Data shown represent the mean ± SEM of two (C), three (A, B, D), and eight (E, F) independent experiments. *$P < .05$, **$P < .01$. Protein bands were determined with rabbit anti-Gal-12 antibody (B, D)

α2,6-linked sialic acid, evidenced by SNA recognition, decreased under hypoxic conditions (Figure 5A). Of note, high mannose glycans (evaluated by ConA binding) were not altered in hypoxia compared to normoxia (Figure 5A). Similar results were observed using the mouse endothelial cell line C166 (data not shown).

To identify potential Gal-12 glycoepitopes on the surface of HUVEC, we next evaluated the presence of sialyl Le^X structures using an anti-CD15s monoclonal antibody. Our results showed that this specific 3-fucosylated glycoepitope was upregulated in response to hypoxic conditions (Figure 5B). Since hypoxia favors the exposure of fucosylated glycans, which serve as potential Gal-12 ligands on the EC surface (Figure 5A,B) and, at the same time, promotes Gal-12 expression in adipocytes (Figure 4C,D), we next evaluated the impact of this lectin in EC biology. We found that Gal-12 bound to HUVEC in a dose and carbohydrate-dependent manner, enhancing EC migration (Figure 5C,D) and promoting formation of tubular structures in vitro tubulogenesis assays (Figure 5E). These effects relied on Gal-12 recognition of fucosylated glycans on HUVEC since 3-FL, but not Lac, abrogated Gal-12-induced EC migration (Figure 5D) and tube formation (Figure 5E). Accordingly, under hypoxic conditions, HUVEC cells were more sensitive to Gal-12-induced tubulogenesis (Figure S4A,B) and this effect was inhibited by 3FL (Figure S4B). Moreover, migration was also induced by mGal-12 in C166 (Figure S4C) and EOMA (data not shown) murine endothelial cells.

Finally, to address the in vivo relevance of Gal-12 in promoting angiogenesis in AT, we examined vascularization of perigonadal AT in WT (*Lgals12*$^{+/+}$) and Gal-12-deficient (*Lgals12*$^{-/-}$) mice. In line with in vitro data, AT from *Lgals12*$^{-/-}$ mice showed a reduced total vascular area (Figure 5F) and lower microvascular density (Figure 5G), when compared to *Lgals12*$^{+/+}$ mice. In addition, vessels from *Lgals12*$^{-/-}$ mice were thinner and evidenced lower branching compared to their WT counterparts (Figure 5H,I), suggesting that Gal-12 contributes not only to vessel

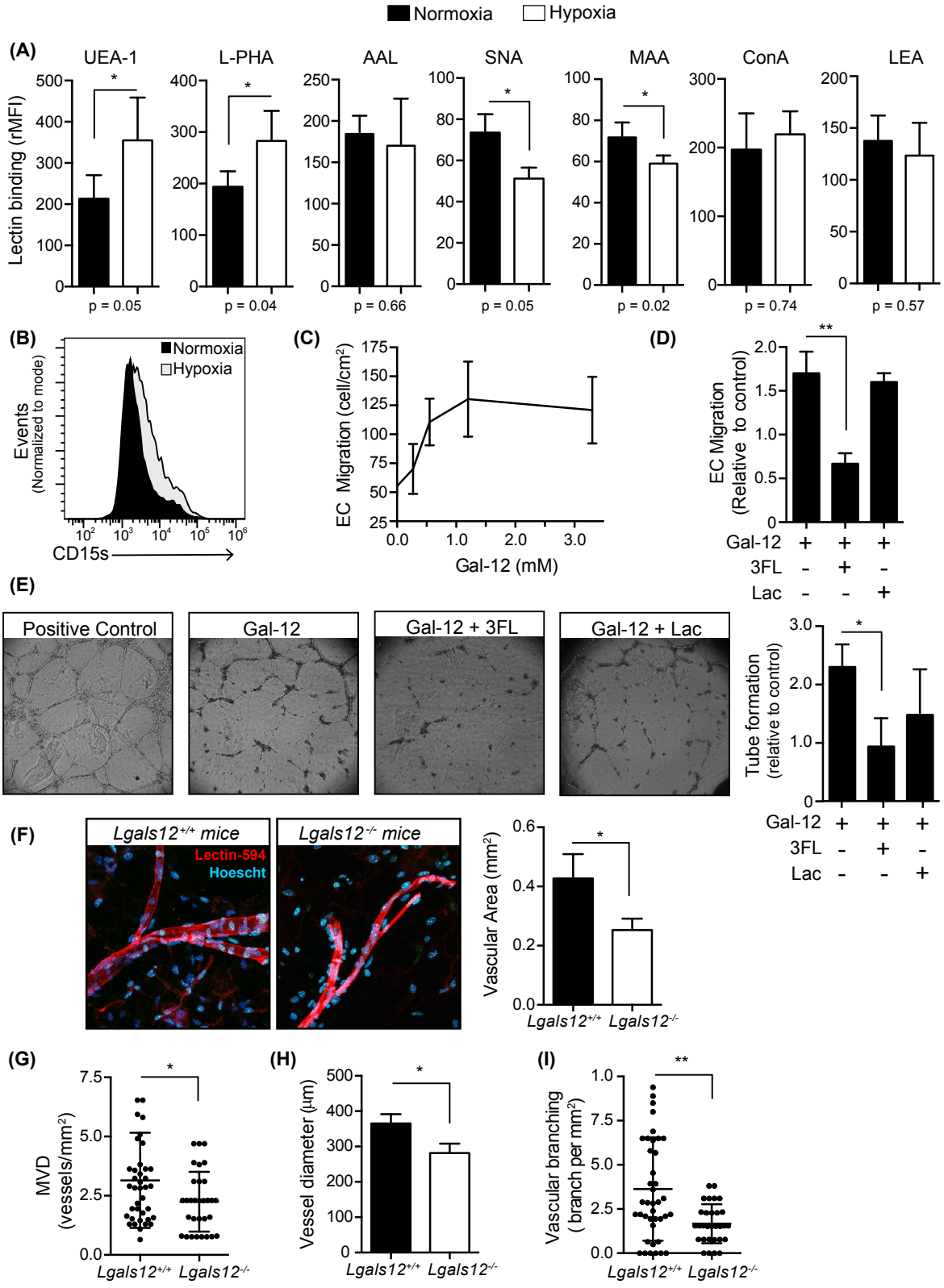

FIGURE 5 Galectin-12 induces angiogenesis through binding to 3-fucosylated glycans. A, Glycophenotyping of HUVEC cultured under normoxic (black) or hypoxic (white) conditions using biotinylated plant lectins by flow cytometry. *Ulex Europaeus* Agglutinin I (UEA-1, 5 μg/mL), L-*Phaseolus vulgaris* (L-PHA, 2 μg/mL), *Aleuria aurantia* lectin (AAL, 2 μg/mL), *Sambucus nigra* lectin (SNA, 2 μg/mL), *Maackia amurensis* lectin II (MAA, 5 μg/mL), Concanavalin A (ConA, 2 μg/mL), and *Lycopersicon esculentum* Lectin (LEA, 2 μg/mL). rMFI (relative mean fluorescence intensity) = (MFI with lectin—MFI without lectin)/MFI without lectin. B, Flow cytometry analysis of CD15s (sialyl Lewis X antigen) expression on the surface of HUVEC under normoxia (black) or hypoxia (white). C,D Migration of HUVEC in the absence or presence of recombinant Gal-12. C, Dose-dependent migration of HUVEC in the presence of increasing concentration of mGal-12. D, Inhibition of Gal-12-induced migration of HUVEC by 3-fucosyllactose (3-FL 0.4 mM) or lactose (Lac, 2 mM). E, Tubulogenesis assay. Left, representative images of Gal-12-induced tubulogenesis by HUVEC. Right, quantification of tubulogenesis assays. Positive control: SFB 15%, VEGF 20 ng/mL and bFGF 20 ng/mL in RPMI medium; Gal-12: 1 μM in SFB 2% in RPMI medium; Gal-12 + 3-FL: 1 μM Gal-12 and 400 μM 3-FL in SFB 2% in RPMI medium; Gal-12 + Lac: 1 μM Gal-12 and 2 mM Lac in SFB 2% in RPMI medium. F-I, In vivo modulation of angiogenesis by endogenous Gal-12. Confocal analysis of vascular architecture of *Lgals12*$^{-/-}$ and *Lgals12*$^{+/+}$ mice after intravital staining. F, Left: representative images of four mice per group perfused with Alexa 594-LEA. Right: Quantification of relative vascular area (vessel area per mm^2 of total AT). G, Microvascular density (MVD = number of microvessels per mm^2). H, Quantification of vessel diameter of AT vasculature. I, vascular branching (expressed as number of branching points per mm^2 of AT). A-F, Bars represent the mean ± SEM of two (B), three (A, F, H) or five (C, D, E) independent experiments. G,I, vessels analyzed are represented in the plot. *$P < .05$ **$P < .01$

formation but also to vessel remodeling. Thus, hypoxia-regulated interactions between Gal-12 and its fucosylated ligands may influence AT vascularization under physiologic or pathologic conditions.

4 | DISCUSSION

Obesity is a complex metabolic disorder linked to diabetic complications, cardiovascular disorders, and malignancies, representing a great threat to global human health. Several lines of evidence indicate that obesity and obesity-associated disorders are connected to pathologic angiogenesis.[45] Given that AT growth is limited by its vascular supply,[46,47] the pro-angiogenic potential of AT depots is critical in limiting their maximal expandability. Consequently, modulation of angiogenesis arises as a novel therapeutic approach.[45,48,49] Testing this hypothesis requires a better understanding of the molecular pathways underlying AT vascularization.

Gal-12 is an unusual member of the galectin family with a dominant expression in adipocytes, sebocytes, and macrophages. This lectin has been shown to control macrophage polarization,[23] adipocyte differentiation,[18] lipid metabolism, and energy balance.[22] The results presented here suggest that Gal-12 might also function as a possible mediator that bridges angiogenesis and AT pathophysiology. Noteworthy, as there was no successful heterologous expression system available for this endogenous lectin, most of its previous functional characterization relied on *Lgals12*$^{-/-}$ mice and/or genetically modified cell lines.[20,22] Here, we report the expression, purification, and biochemical characterization of recombinant mGal-12. In addition, we report an unexpected biochemical feature of this lectin, namely its specific affinity for 3-fucosylated-lactose derivatives, and its new biological function as a regulator of angiogenesis.

Both Gal-12 *in silico* sequence analysis and its localization in LD pointed at a highly hydrophobic structure. Indeed, several attempts to express and purify recombinant Gal-12 with or without an N-terminal His-tag resulted in insoluble protein, or its association to the membrane debris. This last setback was efficiently surpassed by the addition of 0.5% DOC to the lysis buffer and N-terminal His-tagged Gal-12 was obtained in the soluble fraction. Purification of this protein proved challenging, not only because of its natural hydrophobicity but also probably due to a deficient His-tag exposure, as seen in other proteins.[50,51] In the absence of a crystal structure, molecular modeling evidenced five different hydrophobic zones in Gal-12: while hydrophobic zones 2, 3, and 4 are disposed toward the interior of the protein, zones 1 and 5 are highly exposed to the solvent. These hydrophobic patches could be responsible for unsuccessful purification of the His-tagged protein by Ni-NTA columns.[50] Moreover, affinity chromatography with lactose, a canonical ligand for galectins, was also unsuccessful for this lectin, indicating that mGal-12 has very low affinity toward this disaccharide. This unusual feature is probably caused by the absence of several key amino acid residues involved in interactions with this disaccharide (Figure 1). Finally, and based on its unusual high pI, development of a serial anionic/cationic chromatography steps (Figure 2A,B) was key for Gal-12 purification in good yield.

The development of a specific SPA using ASF as ligand and competitive assays with free oligosaccharides as Gal-12 inhibitors pointed at 3-fucosylated glycoepitopes, such as Le^X, as preferred Gal-12 ligands. These findings were subsequently validated by ITC. Thus, results provided by two relevant experimental approaches showed good correlations with theoretical models described. Interestingly, Gal-12-binding specificity for Le^X structures was more closely related to glycan-binding preferences of DC-SIGN, a C-type lectin receptor, than that corresponding to the galectin family.[52] Indeed,

Gal-12 is the first reported galectin, which preferentially recognizes 3-fucosylated structures, as fucosylation of the 3 –OH group of glucose appeared to be disruptive to other galectins, due to the requirement of a free 3 –OH group on Glc/GlcNAc for binding.[43,53]

Since no experimental structure for full-length Gal-12 has been reported yet, homology models represented useful tools for studying the atomistic determinants responsible for recognition of 3-fucosylated glycans; however, they should be considered only as indicative frameworks useful for identifying residues involved in ligand binding, considering that mGal-12 structure has not been solved experimentally. When compared to homology modeling performed for other proteins,[54,55] the low percentage obtained for the C-terminal CRD may likely be associated to its high divergence from the galectin consensus sequence.[20] In spite of these low percentages of identity, reasonable Modeller scores were obtained, and further molecular docking allowed interpretation of the experimental results obtained for mGal-12-ligand interactions, providing good correlation with the SPA and ITC data (see supporting information Figure S2B). Indeed, the Gal-12 N-terminal CRD model was essential for identifying Arg^{73} as the key residue involved in hydrogen bond interactions with 3-fucosylated glycans, as previously described for a fucolectin, the *Anguilla anguilla* agglutinin.[56] Notably, in other members of the galectin family, this residue is a highly conserved His that is crucial for Lac recognition.[5] Interestingly, the presence of Arg^{73} could also explain the observed low binding affinity of mGal-12 for lactose, as shown by unsuccessful purification on lactosyl-Sepharose columns and by solid phase/ITC assays. Of note, mGal-12 clearly differs from hGal-12 in this matter, as the latter was purified using a lactose-resin.[20] Differences in the LBG may explain this disparity: while mGal-12N lacks two of the seven key amino acid residues that define the lactose binding family, hGal-12N presents all seven of them. Further analysis and crystallization of both orthologs complexed with ligands will help understand these differences. On the other hand, the C-terminal CRD model showed a trend toward lower binding affinities than Gal-12N (Table 3), as described for other tandem-repeat type galectins such as Gal-8.[42] The correlation of computational and biochemical data suggests that the N-terminal domain of mGal-12 is mainly responsible for the preferential ligand-binding activity observed. Considering the high hydrophobicity of mGal-12 and its selective compartmentalization in LDs, glycolipids could also serve as potential ligands for this lectin, as described for other tandem-type galectins.[57-59] Though no glycolipid partners for Gal-12 have been documented to date, VPS13C, a major Gal-12-binding protein required for its stability,[60] was recently identified as a lipid transporter between the ER and other organelles.[61]

The biochemical and biophysical characterization of Gal-12 structure and the identification of its preferred carbohydrate ligands allowed delving into new biological roles of this protein, and revealed a previously unanticipated function of this protein closely related to the AT remodeling process. As reiterative expansion and reduction in AT size throughout adult lifespan requires concomitant changes in the microvasculature,[45,46,62] we sought to characterize the role of Gal-12 in the angiogenic process. Notably, other members of this family such as Gal-1,[38,63,64], Gal-3,[65,66] Gal-8,[67] and Gal-9[68] have already shown pro-angiogenic roles. Of note, mGal12 is able to induce endothelial cell migration both in HUVEC and in murine endothelial cells, indicating that despite the low homology between mGal12 and hGal12, the glycan-binding features are conserved. We have also demonstrated a similar behavior for human Gal-1, as immunosuppressive stimuli favor a permissive glycophenotype on both HUVEC and EOMA cells, while proinflammatory signals reduce expression of these glyco-epitopes in both cell lines.[64]

Interestingly, we found that adipocytes upregulate Gal-12 expression under hypoxic conditions and Gal-12 ligands are considerably increased in ECs under hypoxia. Moreover, we found that Gal-12 promoted cell migration and induced formation of tubular-like structures on HUVEC through interaction with fucosylated glycans. Thus, hypoxia may fuel Gal-12 activity both by increasing its expression in adipocytes and by favoring the availability of fucosylated glycans on ECs. Finally, we found that AT from *Lgals12*$^{-/-}$ mice exhibited a reduced vascular network than that found in their WT counterparts (Figure 5). In this context, the impact of different factors in AT angiogenesis has been previously evaluated in other transgenic mouse models, either in nutritionally induced obesity or in elder mice under standard diet. In this regard, inactivation of placental growth factor (PIGF) impaired AT angiogenesis, as evidenced by reduced blood vessel size in gonadal AT of *Pigf*$^{-/-}$ mice with both standard-fat and high-fat diet.[69] In addition, loss of neuregulin-4 caused reduction in perigonadal AT blood vessels in 20-week-old-mice fed with normal chow.[70] Herein, the effect of Gal-12 deficiency on AT angiogenesis was evident even in young animals under standard diet; yet, the impact of reduced vascularization on AT development under different nutritional or inflammatory states deserves further evaluation. Of note, *Lgals12*$^{-/-}$ animals exhibited substantially reduced perigonadal AT, despite normal body weight.[22]

In summary, our results highlight a central role for Gal-12 as a potential mediator supporting AT expansion through promotion of vascular supply. Inhibition of Gal-12-mediated angiogenesis by 3-fucosylated glycans highlights the relevance of carbohydrate recognition in Gal-12 functions, and suggests new strategies to control AT vascularization by modulating Gal-12-glycan interactions. Further identification of possible

Gal-12 target molecules on ECs will be critical to further dissect the molecular mechanisms underlying this effect.

In addition to adipocytes, ECs, and inflammatory cells, growing AT involves adipose-derived stromal cells that influence the AT vascular niche by expressing pro-angiogenic molecules and directly contributing to new blood vessel formation.[46,49] The possible role of Gal-12 in stromal cell function deserves further studies. Importantly, all mentioned cell types reciprocally interact within the AT microenvironment through generation of several pro-angiogenic factors, adipokines, and cytokines, to regulate angiogenesis.[45,49]

Finally, local hypoxia has been proposed to be a critical mechanism leading to dysregulation of AT function in the context of obesity through activation of inflammatory pathways causing insulin resistance and impaired lipid storage.[71-74] Accordingly, augmented Gal-12 expression under hypoxic conditions may contribute not only to TA angiogenesis but might also provide an alternative explanation for activation of pro-inflammatory pathways[23] and impaired insulin sensitivity and lipolysis[22,23] induced by this lectin. Thus, through modulation of adipocytes, ECs, and/or inflammatory cells, Gal-12 may function as a key modulator of AT metabolism with critical implications in AT immunological and endocrinological switch following nutritional imbalance.

ACKNOWLEDGMENTS

AJC, JMPS, LIP, LS, VS, DOC, SDL, GAR, and KVM are researchers from Consejo Nacional de Investigaciones Científicas y Técnicas (CONICET), Argentina. SMM was supported by a doctoral fellowship from CONICET. This work was supported by grants from Sales, Bunge & Born and René Baron Foundations (Argentina) and The Richard Lounsbery Foundation (USA) (to GAR), as well as grants from Agencia Nacional de Promoción Científica y Tecnológica (ANPCyT, grant PICT 2015-0564 to KVM, PICT V 2014-3687 to GAR and PICT 2016-0205 to DOC) as well as from University of Buenos Aires to GAR (20020120100276; 2013-2015). We thank Prof. Darío A. Estrin (INQUIMAE - CONICET/UBA) for access to cluster facilities and Mercedes Goin and Federico Carrizo for advice on bacterial culture and ion exchange resins.

CONFLICT OF INTEREST

No conflict of interest has been declared by the authors.

AUTHOR CONTRIBUTIONS

S. Di Lella, D.O. Croci, V. Sundblad, G.A. Rabinovich, and K.V. Mariño designed and conceptualized the study. S.M. Maller, A.J. Cagnoni, and J.M. Pérez Sáez purified and characterized Gal-12. S.M. Maller and J.M. Pérez Sáez generated in house rat anti-Gal-12 polyclonal antibodies. S.M. Maller, L. Sigaut, and L.I. Pietrasanta designed, performed, and analyzed microscopy experiments. S.M. Maller, N. Bannoud, and D.O. Croci designed and performed angiogenesis experiments. S.M. Maller, A.J. Cagnoni, and S. Di Lella carried out computational studies. S.M. Maller, A.J. Cagnoni, N. Bannoud, S. Di Lella, V. Sundblad, L. Sigaut, L.I. Pietrasanta, D.O. Croci, G.A. Rabinovich, and K.V. Mariño analyzed and interpreted data. S.M. Maller, A.J. Cagnoni, S. Di Lella, L. Sigaut, L.I. Pietrasanta, D.O. Croci, V. Sundblad, G.A. Rabinovich, and K.V. Mariño drafted the article and revised it critically. R.-Y. Yang and F.-T. Liu provided *Lgals12*$^{-/-}$ mice and Gal-12 constructs and revised the manuscript critically.

REFERENCES

1. Grant RW, Dixit VD. Adipose tissue as an immunological organ. *Obesity (Silver Spring)*. 2015;23:512-518.
2. Grant R, Youm Y-H, Ravussin A, Dixit VD. Quantification of adipose tissue leukocytosis in obesity. *Methods Mol Biol*. 2013;1040:195-209.
3. Reilly SM, Saltiel AR. Adapting to obesity with adipose tissue inflammation. *Nat Rev Endocrinol*. 2017;13:633-643.
4. Cao Y. Angiogenesis and vascular functions in modulation of obesity, adipose metabolism, and insulin sensitivity. *Cell Metab*. 2013;18:478-489.
5. Vasta GR. Galectins as pattern recognition receptors: structure, function, and evolution. *Adv Exp Med Biol*. 2012;946:21-36.
6. Rabinovich GA, Toscano MA. Turning "sweet" on immunity: galectin-glycan interactions in immune tolerance and inflammation. *Nat Rev Immunol*. 2009;9:338-352.
7. Croci DO, Cerliani JP, Pinto NA, Morosi LG, Rabinovich GA. Regulatory role of glycans in the control of hypoxia-driven angiogenesis and sensitivity to anti-angiogenic treatment. *Glycobiology*. 2014;24:1283-1290.
8. Cerliani JP, Blidner AG, Toscano MA, Croci DO, Rabinovich GA. Translating the "Sugar Code" into immune and vascular signaling programs. *Trends Biochem Sci*. 2017;42:255-273.
9. Rabinovich GA, Toscano MA, Jackson SS, Vasta GR. Functions of cell surface galectin-glycoprotein lattices. *Curr Opin Struct Biol*. 2007;17:513-520.
10. Liu F-T, Patterson RJ, Wang JL. Intracellular functions of galectins. *Biochim Biophys Acta*. 2002;1572:263-273.
11. Hirabayashi J, Kasai K. The family of metazoan metal-independent beta-galactoside-binding lectins: structure, function and molecular evolution. *Glycobiology*. 1993;3:297-304.
12. Cagnoni AJ, Perez Saez JM, Rabinovich GA, Marino KV. Turning-off signaling by siglecs, selectins, and galectins: chemical inhibition of glycan-dependent interactions in cancer. *Front Oncol*. 2016;6:109.
13. Dam TK, Brewer CF. Lectins as pattern recognition molecules: the effects of epitope density in innate immunity. *Glycobiology*. 2010;20:270-279.
14. Dam TK, Brewer CF. Maintenance of cell surface glycan density by lectin-glycan interactions: a homeostatic and innate immune regulatory mechanism. *Glycobiology*. 2010;20:1061-1064.

15. Nio-Kobayashi J. Tissue- and cell-specific localization of galectins, β-galactose-binding animal lectins, and their potential functions in health and disease. *Anat Sci Int*. 2016;92:25-36.
16. Sundblad V, Morosi LG, Geffner JR, Rabinovich GA. Galectin-1: a jack-of-all-trades in the resolution of acute and chronic inflammation. *J Immunol*. 2017;199:3721-3730.
17. Ilarregui JM, Bianco GA, Toscano MA, Rabinovich GA. The coming of age of galectins as immunomodulatory agents: impact of these carbohydrate binding proteins in T cell physiology and chronic inflammatory disorders. *Ann Rheum Dis.* 2005;64(suppl_4):iv96–iv103.
18. Yang R-Y, Hsu DK, Yu L, Chen H-Y, Liu F-T. Galectin-12 is required for adipogenic signaling and adipocyte differentiation. *J Biol Chem*. 2004;279:29761-29766.
19. Hotta K, Funahashi T, Matsukawa Y, et al. Galectin-12, an adipose-expressed galectin-like molecule possessing apoptosis-inducing activity. *J Biol Chem*. 2001;276:34089-34097.
20. Yang RY, Hsu DK, Yu L, Ni J, Liu FT. Cell cycle regulation by galectin-12, a new member of the galectin superfamily. *J Biol Chem*. 2001;276:20252-20260.
21. Fasshauer M, Klein J, Lossner U, Paschke R. Negative regulation of adipose-expressed galectin-12 by isoproterenol, tumor necrosis factor alpha, insulin and dexamethasone. *Eur J Endocrinol*. 2002;147:553-559.
22. Yang R-Y, Yu L, Graham JL, et al. Ablation of a galectin preferentially expressed in adipocytes increases lipolysis, reduces adiposity, and improves insulin sensitivity in mice. *Proc Natl Acad Sci USA*. 2011;108:18696-18701.
23. Wan L, Lin H-J, Huang C-C, et al. Galectin-12 enhances inflammation by promoting M1 polarization of macrophages and reduces insulin sensitivity in adipocytes. *Glycobiology*. 2016;26:732-744.
24. Eswar N, Webb B, Marti-Renom MA, et al. Comparative protein structure modeling using modeller. *Curr Protoc Bioinforma*. 2006;15(1):5-6.
25. Marti-Renom MA, Stuart AC, Fiser A, Sanchez R, Melo F, Sali A. Comparative protein structure modeling of genes and genomes. *Annu Rev Biophys Biomol Struct*. 2000;29:291-325.
26. Fiser A, Do RK, Sali A. Modeling of loops in protein structures. *Protein Sci*. 2000;9:1753-1773.
27. Humphrey W, Dalke A, Schulten K. VMD: visual molecular dynamics. *J Mol Graph*. 1996;14(27-28):33-38.
28. Case DA, Babin V, Berryman JT, et al. *AMBER14*. San Francisco: University of California; 2014.
29. Berendsen HJC, Postma JPM, van Gunsteren WF, DiNola A, Haak JR. Molecular-dynamics with coupling to an external bath. *J Chem Phys*. 1984;81:3684-3690.
30. van Gunsteren WF, Berendsen HJC. Computer simulation of molecular dynamics: methodology, applications, and perspectives in chemistry. *Angew Chemie Int Ed English*. 1990;29:992-1023.
31. Hornak V, Abel R, Okur A, Strockbine B, Roitberg A, Simmerling C. Comparison of multiple Amber force fields and development of improved protein backbone parameters. *Proteins*. 2006;65:712-725.
32. Hanwell MD, Curtis DE, Lonie DC, Vandermeersch T, Zurek E, Hutchison GR. Avogadro: an advanced semantic chemical editor, visualization, and analysis platform. *J Cheminform*. 2012;4:17.
33. Trott O, Olson AJ. AutoDock Vina: improving the speed and accuracy of docking with a new scoring function, efficient optimization, and multithreading. *J Comput Chem*. 2010;31:455-461.
34. Seeliger D, de Groot BL. Ligand docking and binding site analysis with PyMOL and Autodock/Vina. *J Comput Aided Mol Des*. 2010;24:417-422.
35. Rabinovich G, Castagna L, Landa C, Riera CM, Sotomayor C. Regulated expression of a 16-kd galectin-like protein in activated rat macrophages. *J Leukoc Biol*. 1996;59:363-370.
36. Rapoport EM, Pochechueva TV, Kurmyshkina OV, et al. Solid-phase assays for study of carbohydrate specificity of galectins. *Biochem (Mosc)*. 2010;75:310-319.
37. Rubin CS, Hirsch A, Fung C, Rosen OM. Development of hormone receptors and hormonal responsiveness in vitro. Insulin receptors and insulin sensitivity in the preadipocyte and adipocyte forms of 3T3-L1 cells. *J Biol Chem*. 1978;253:7570-7578.
38. Croci DO, Salatino M, Rubinstein N, et al. Disrupting galectin-1 interactions with N-glycans suppresses hypoxia-driven angiogenesis and tumorigenesis in Kaposi's sarcoma. *J Exp Med*. 2012;209:1985-2000.
39. Schindelin J, Arganda-Carreras I, Frise E, et al. Fiji: an open-source platform for biological-image analysis. *Nat Methods*. 2012;9:676-682.
40. Meynier C, Guerlesquin F, Roche P. Computational studies of human galectin-1: role of conserved tryptophan residue in stacking interaction with carbohydrate ligands. *J Biomol Struct Dyn*. 2009;27:49-58.
41. Ahmad N, Gabius H-J, Sabesan S, Oscarson S, Brewer CF. Thermodynamic binding studies of bivalent oligosaccharides to galectin-1, galectin-3, and the carbohydrate recognition domain of galectin-3. *Glycobiology*. 2004;14:817-825.
42. Carlsson S, Oberg CT, Carlsson MC, et al. Affinity of galectin-8 and its carbohydrate recognition domains for ligands in solution and at the cell surface. *Glycobiology*. 2007;17:663-676.
43. Hirabayashi J, Hashidate T, Arata Y, et al. Oligosaccharide specificity of galectins: a search by frontal affinity chromatography. *Biochim Biophys Acta*. 2002;1572:232-254.
44. Bum-Erdene K, Leffler H, Nilsson UJ, Blanchard H. Structural characterisation of human galectin-4 N-terminal carbohydrate recognition domain in complex with glycerol, lactose, 3′-sulfo-lactose, and 2′-fucosyllactose. *Sci Rep*. 2016;6:20289.
45. Cao Y. Angiogenesis modulates adipogenesis and obesity. *J Clin Invest*. 2007;117:2362-2368.
46. Christiaens V, Lijnen HR. Angiogenesis and development of adipose tissue. *Mol Cell Endocrinol*. 2010;318:2-9.
47. Corvera S, Gealekman O. Adipose tissue angiogenesis: impact on obesity and type-2 diabetes. *Biochim Biophys Acta*. 2014;1842:463-472.
48. Lijnen HR. Angiogenesis and obesity. *Cardiovasc. Res*. 2008;78:286-293.
49. Cao Y. Adipose tissue angiogenesis as a therapeutic target for obesity and metabolic diseases. *Nat Rev Drug Discov*. 2010;9:107-115.
50. Hefti MH, Vugt-Van V, der Toorn CJ, Dixon R, Vervoort J. A novel purification method for histidine-tagged proteins containing a thrombin cleavage site. *Anal Biochem*. 2001;295:180-185.
51. Rubio I, Combita AL, Ortiz-Reyes B, Navas M-C. Hepatitis C virus core protein production and purification in a baculovirus expression system for biological assays. *Biomedica*. 2005;25:34-45.
52. Garcia-Vallejo JJ, van Kooyk Y. DC-SIGN: the strange case of Dr. Jekyll and Mr. Hyde. *Immunity*. 2015;42(6):983-985.
53. Noll AJ, Gourdine J-P, Yu Y, Lasanajak Y, Smith DF, Cummings RD. Galectins are human milk glycan receptors. *Glycobiology*. 2016;26:655-669.

54. Katiyar A, Lenka SK, Lakshmi K, Chinnusamy V, Bansal KC. In silico characterization and homology modeling of thylakoid bound ascorbate peroxidase from a drought tolerant wheat cultivar. *Genomics, Proteomics & Bioinformatics*. 2009;7(4):185-193.
55. Guardia CMA, Gauto DF, Di Lella S, Rabinovich GA, Marti MA, Estrin DA. An integrated computational analysis of the structure, dynamics, and ligand binding interactions of the human galectin network. *J Chem Inf Model*. 2011;51:1918-1930.
56. Bianchet MA, Odom EW, Vasta GR, Amzel LM. A novel fucose recognition fold involved in innate immunity. *Nat Struct Biol*. 2002;9:628-634.
57. Ideo H, Seko A, Ishizuka I, Yamashita K. The N-terminal carbohydrate recognition domain of galectin-8 recognizes specific glycosphingolipids with high affinity. *Glycobiology*. 2003;13:713-723.
58. Danielsen EM, Hansen GH. Lipid rafts in epithelial brush borders: atypical membrane microdomains with specialized functions. *Biochim Biophys Acta*. 2003;1617:1-9.
59. Delacour D, Gouyer V, Zanetta J-P, et al. Galectin-4 and sulfatides in apical membrane trafficking in enterocyte-like cells. *J Cell Biol*. 2005;169:491-501.
60. Yang R-Y, Xue H, Yu L, Velayos-Baeza A, Monaco AP, Liu F-T. Identification of VPS13C as a galectin-12-binding protein that regulates galectin-12 protein stability and adipogenesis. *PLoS One*. 2016;11:e0153534.
61. Kumar J, Kline NL, Masison DC. Human DnaJB6 antiamyloid chaperone protects yeast from polyglutamine toxicity separately from spatial segregation of aggregates. *Mol Cell Biol*. 2018;38(23):e00437-18.
62. Rodrigues T, Matafome P, Seica R. A vascular piece in the puzzle of adipose tissue dysfunction: mechanisms and consequences. *Arch Physiol Biochem*. 2014;120:1-11.
63. Thijssen VL, Barkan B, Shoji H, et al. Tumor cells secrete galectin-1 to enhance endothelial cell activity. *Cancer Res*. 2010;70:6216-6224.
64. Croci DO, Cerliani JP, Dalotto-Moreno T, et al. Glycosylation-dependent lectin-receptor interactions preserve angiogenesis in anti-VEGF refractory tumors. *Cell*. 2014;156:744-758.
65. Markowska AI, Liu F-T, Panjwani N. Galectin-3 is an important mediator of VEGF- and bFGF-mediated angiogenic response. *J Exp Med*. 2010;207:1981-1993.
66. Markowska AI, Jefferies KC, Panjwani N. Galectin-3 protein modulates cell surface expression and activation of vascular endothelial growth factor receptor 2 in human endothelial cells. *J Biol Chem*. 2011;286:29913-29921.
67. Delgado VMC, Nugnes LG, Colombo LL, et al. Modulation of endothelial cell migration and angiogenesis: a novel function for the "tandem-repeat" lectin galectin-8. *FASEB J*. 2011;25:242-254.
68. Aanhane E, Schulkens IA, Heusschen R, et al. Different angioregulatory activity of monovalent galectin-9 isoforms. *Angiogenesis*. 2018;21:545-555.
69. Lijnen HR, Christiaens V, Scroyen I, et al. Impaired adipose tissue development in mice with inactivation of placental growth factor function. *Diabetes*. 2006;55:2698-2704.
70. Nugroho DB, Ikeda K, Barinda AJ, et al. Neuregulin-4 is an angiogenic factor that is critically involved in the maintenance of adipose tissue vasculature. *Biochem Biophys Res Commun*. 2018;503:378-384.
71. Galic S, Oakhill JS, Steinberg GR. Adipose tissue as an endocrine organ. *Mol Cell Endocrinol*. 2010;316:129-139.
72. Guilherme A, Virbasius JV, Puri V, Czech MP. Adipocyte dysfunctions linking obesity to insulin resistance and type 2 diabetes. *Nat Rev Mol Cell Biol*. 2008;9:367-377.
73. Rutkowski JM, Davis KE, Scherer PE. Mechanisms of obesity and related pathologies: the macro- and microcirculation of adipose tissue. *FEBS J*. 2009;276:5738-5746.
74. Tilg H, Moschen AR. Adipocytokines: mediators linking adipose tissue, inflammation and immunity. *Nat Rev Immunol*. 2006;6:772-783.
75. Waterhouse AM, Procter JB, Martin DMA, Clamp M, Barton GJ. Jalview Version 2—a multiple sequence alignment editor and analysis workbench. *Bioinformatics*. 2009;25:1189-1191.

SUPPORTING INFORMATION

Additional supporting information may be found online in the Supporting Information section.

How to cite this article: Maller SM, Cagnoni AJ, Bannoud N, et al. An adipose tissue galectin controls endothelial cell function via preferential recognition of 3-fucosylated glycans. *The FASEB Journal*. 2020;34:735–753. https://doi.org/10.1096/fj.201901817R